Seasonal, Regional, and Storm-Scale Variability of Cloud-to-Ground Lightning Characteristics in Florida

SCOTT D. RUDLOSKY AND HENRY E. FUELBERG

Department of Earth, Ocean, and Atmospheric Science, The Florida State University, Tallahassee, Florida

(Manuscript received 6 August 2010, in final form 29 October 2010)

ABSTRACT

Seasonal, regional, and storm-scale variations of cloud-to-ground (CG) lightning characteristics in Florida are presented. Strong positive CG (+CG) and negative CG (−CG) flashes (i.e., having large peak current) are emphasized since they often are associated with strong storms, structural damage, and wildfire ignitions. Although strong −CG flashes are most common during the warm season (May–September) over the peninsula, the greatest proportion of strong +CG flashes occurs during the cool season (October–April) over the panhandle. The warm season exhibits the smallest +CG percentage but contains the greatest +CG flash densities, due in part to more ambiguous +CG reports (15–20 kA). The more frequent occurrence of ambiguous +CG reports helps explain the unusually small average +CG peak current during the warm season, whereas strong +CG reports (>20 kA) appear to be responsible for the greater average warm season +CG multiplicity. The −CG flash density, multiplicity, and peak current appear to be directly related, exhibiting their greatest values during the warm season when deep storms are most common. A case study examines the atmospheric conditions and storm-scale processes associated with two distinct groups of storms on 13–14 May 2007. Although these groups of storms form in close proximity, several factors combine to produce predominately strong +CG and −CG flashes in the northern (south Georgia) and southern (north Florida) regions, respectively. Results suggest that heat and smoke very near preexisting wildfires are key ingredients in producing reversed-polarity (+CG dominated) storms that often ignite subsequent wildfires.

1. Introduction

Cloud-to-ground (CG) lightning distributions are strongly influenced by seasonal and regional variations in atmospheric conditions. Thus, analysis of CG characteristics and their relation to specific changes in atmospheric conditions can help to better define the CG threat. Many studies have described CG variability on both the seasonal and regional scales; however, ambiguity still remains in the relationships between atmospheric conditions, storm-scale processes, and CG characteristics. Rudlosky and Fuelberg (2010) presented regional CG distributions following the most recent major upgrade of the National Lightning Detection Network (NLDN). Postupgrade (2004–09) results confirmed the findings of several preupgrade studies (e.g., Lyons et al. 1998a; Orville and Huffines 2001) that regional CG patterns are highly dependent on both the meteorological variability and NLDN detection capabilities. Rudlosky and Fuelberg (2010) also noted that seasonal variability must be examined to better define apparent relationships between storm properties and lightning production, but that seasonal differences were best described on the regional scale.

Although CG flashes are predominately negative, they sometimes lower positive charge to ground. The percentage of positive CG (+CG) flashes has been shown to vary both seasonally and regionally (e.g., Orville and Huffines 2001). Physical differences between +CG and negative CG (−CG) flashes can be attributed to the properties of their individual components (i.e., return strokes; Saba et al. 2006). These CG properties control the amount of charge that is neutralized and damage caused, since the polarity, multiplicity (number of return strokes), peak current, and continuing current (CC) are related to the amount and type of charge that is available within an individual thunderstorm (e.g., Saba et al. 2006). Both +CG and −CG flashes can exhibit CC, which is the most critical lightning parameter for igniting wildfires

Corresponding author address: Scott D. Rudlosky, EOAS—Meteorology, The Florida State University, P.O. Box 3064520, Tallahassee, FL 32306-4520.
E-mail: srudlosky@fsu.edu

DOI: 10.1175/2010MWR3585.1

© 2011 American Meteorological Society

(Latham and Williams 2001). However, Saba et al. (2010, manuscript submitted to *J. Geophys. Res.*, hereafter S10) found that 75% of +CG flashes contain at least one long continuing current (LCC; >40 ms) event, while only 30% of −CG flashes do so. Although the NLDN does not measure CC directly, several studies have examined relationships between CC and measured CG properties (e.g., Krehbiel et al. 1979; Brook et al. 1982; Rakov et al. 1994; Saba et al. 2006).

The polarity of CG flashes strongly influences their threat to vulnerable infrastructure and their likelihood to ignite wildfires (e.g., Rakov and Uman 2003, p. 214). Positive CG flashes typically contain a single return stroke, exhibit the greatest peak currents (sometimes near 300 kA), and produce the largest charge transfers to ground (Rakov 2003). The combination of large peak current and LCC is unique to +CG flashes (Saba et al. 2006) and is likely responsible for the increased damage and wildfire ignitions that have been associated with +CG flashes (e.g., Latham and Williams 2001; Rakov and Uman 2003, p. 214). Conversely, Saba et al. (2006) found that it is highly unlikely for −CG return strokes to contain both peak current greater than 20 kA and CCs longer than 40 ms (i.e., LCC). The overwhelming majority of LCCs in −CG flashes are initiated by subsequent strokes of multistroke flashes, as opposed to the first stroke of multistroke flashes or the only stroke of single-stroke flashes (Rakov et al. 1994). Furthermore, Biagi et al. (2007) found LCC in a large fraction of low peak current −CG return strokes.

Positive CG can dominate −CG under certain conditions (e.g., Orville and Silver 1997). The local mesoscale environment indirectly influences CG polarity by directly controlling storm structure, dynamics, and microphysics, and in turn, storm electrification (Carey and Buffalo 2007). Some storms produce predominately +CG flashes for extended periods of time (MacGorman and Burgess 1994); however, regions with a relatively moist troposphere experience fewer +CG-dominated storms (Knapp 1994). Williams et al. (2005) noted a general absence of +CG-dominated storms in Florida; however, they presented a counterexample of a severe storm that produced predominately +CG flashes during a 40-min period. They noted that large surface dewpoint depressions and high cloud bases may have enhanced the +CG production, but that nearby wildfires made it difficult to determine the relative roles of thermodynamics and aerosols as the cause for the enhanced +CG production (Williams et al. 2005). The case study herein (section 3c) documents a similar scenario near the Okefenokee Swamp during 13–14 May 2007. Our goal is to examine the influence of atmospheric conditions on the storm-scale processes that lead to the enhanced production of strong +CG flashes.

Many studies have suggested that both drier environments (higher cloud bases; Carey and Buffalo 2007) and smoke ingestion (Williams et al. 2005; Lang and Rutledge 2006) are related to a reversal of the non-inductive charging mechanism and increased +CG production. In these reversed-polarity (+CG dominated) storms, smoke related cloud condensation nuclei (CCN) likely result in smaller droplets that ascend rapidly in strong updrafts, thereby suppressing precipitation processes in the lower levels and allowing greater supercooled water content in the mixed phase region (Rosenfeld et al. 2007). Dry conditions typically lead to broad updrafts (scaled by higher cloud bases) that result in less entrainment, greater updraft speeds, and faster collision velocities, which can cause reversed-polarity charging in the mixed phase region (e.g., Carey and Buffalo 2007). This combination of factors previously has been associated with storms that produce many strong +CG flashes (e.g., Lang and Rutledge 2006). Since strong +CG flashes generally have a CC component associated with large charge transfer, they are prime candidates for igniting wildfires (e.g., Fuquay et al. 1972). Thus, our case study also examines the polarity of CG flashes near natural wildfire ignitions on 13–14 May 2007.

Many questions remain concerning the occurrence and distribution of weak (10–15 kA) and ambiguous (15–20 kA) +CG reports. Cummins et al. (1998) first documented the tendency for the NLDN to misclassify some intracloud (IC) discharges as low-amplitude +CG reports. More recently, Cummins and Murphy (2009) suggested that +CG discharges with estimated peak current I_p between 10–20 kA are a mixture of IC and CG pulses. These reports are abundant in the Southeast because of the NLDN's increased sensitivity due to shorter baseline distances between sensors (Orville and Huffines 2001). Surprisingly, Rudlosky and Fuelberg (2010) noted that regions with mostly strong +CG flashes (>20 kA) exhibit small average +CG multiplicity (e.g., the Great Plains), whereas regions with many ambiguous +CG reports (15–20 kA) exhibit unusually large average +CG multiplicity (e.g., the Southeast). Most previous studies have removed +CG reports with I_p less than 10 kA; however, based on recent findings by Biagi et al. (2007) we removed those with I_p less than 15 kA, except in our weak +CG analysis. The weak +CG analysis compares the distributions of weak +CG (10–15 kA), ambiguous +CG (15–20 kA), and strong +CG (>20 kA) reports during 2002–06. Data availability restricted our weak +CG analysis to years prior to 2006 (section 2).

The greatest annual flash densities in the United States occur in Florida (e.g., Hodanish et al. 1997; Orville and Huffines 2001; Rudlosky and Fuelberg 2010). Florida's geography, its juxtaposition with several bodies of water,

and seasonal changes in atmospheric forcing, produce significant spatial and temporal variability in its CG flash distribution (Hodanish et al. 1997). Interactions between synoptic (e.g., squall lines) and mesoscale (e.g., the sea breeze) systems strongly influence the location and magnitude of Florida's CG maxima and minima (Hodanish et al. 1997), resulting in considerable seasonal and regional variability. Florida also represents a particularly challenging region for the NLDN since its geography constrains the number and spacing of NLDN sensors (Cummins and Murphy 2009). Florida's CG patterns are unique because of its abundance of flashes, strong seasonal and regional variability, and constraints on NLDN sensor distributions. Therefore, the present study examines Florida's seasonal, regional, and storm-scale CG variability during 2004–09.

Florida's greatest CG flash densities occur during the warm season (May–September) when thunderstorm activity is modulated on the mesoscale by sea-breeze convergence lines that develop almost daily on one or both coasts (e.g., López and Holle 1986). Warm season CG patterns are due to complex interactions between the sea-breeze circulation, the shape of the coastline, and the prevailing low-level flow (López and Holle 1986; Arritt 1993; Reap 1994; Lericos et al. 2002). Diurnally forced storms produce the majority of warm season CG flashes in the Southeast and exhibit relatively small +CG percentages (Zajac and Rutledge 2001). Since the total CG flash rate increases dramatically with cloud depth (Williams 1985) and −CG flashes are more prevalent in deep clouds (e.g., Kopp and Orville 1987; Engholm et al. 1990; Rakov 2003), Florida's warm season exhibits the minimum +CG percentage.

Synoptic-scale systems dominate Florida's cool season CG production (October–April), when CG flash densities are a minimum and mainly are produced by mesoscale convective systems (MCSs) that often are associated with midlatitude frontal systems (e.g., Hodanish et al. 1997; Zajac and Rutledge 2001). Zajac and Rutledge (2001) found that MCSs (e.g., squall lines) were characterized by a relatively large +CG percentage and +CG I_p. Greater cool season +CG percentages also have been associated with increased wind shear (e.g., Brook et al. 1982), elevated cloud bases (e.g., Williams et al. 2005), and shallower warm cloud depth (e.g., Engholm et al. 1990).

Our objective is to document the seasonal, regional, and storm-scale variability of CG characteristics in Florida. We seek to improve our understanding of the relationships between atmospheric conditions, storm-scale processes, and CG characteristics to better define the CG threat. Discussions about the physical mechanisms leading to the observed CG patterns seek to identify those factors that indicate an increased likelihood of severe weather, structural damage, and/or wildfire ignition.

2. Data and methods

The CG data used in our study were collected by the NLDN that is owned and operated by Vaisala Inc. Our NLDN dataset reports the location, time, polarity, and I_p of the first CG return stroke, as well as the multiplicity of each CG flash. The 2002–03 upgrade resulted in a stroke detection efficiency (DE) of 60%–80%, a flash DE of 90%–95%, and a location accuracy better than 500 m (Cummins and Murphy 2009). Six years of CG data (2004–09) were examined, with our domain including parts of Alabama and Georgia, plus all of Florida and its surrounding coastal waters (Fig. 1). Readers should note that the present study only examines the I_p of the first return stroke and that +CG flashes are defined by I_p greater than 15 kA, except for the analysis of weak +CG reports.

Geographical Information System (GIS) software was used to create a 5 km × 5 km grid and to assign all CG flashes to the grid cell of their occurrence. Grids of monthly composite flash density were combined in GIS to create seasonal flash density maps. Final grids included total CG, −CG, and +CG flash densities (flashes per square kilometer per month) for both the warm and cool seasons. Rudlosky and Fuelberg (2010) emphasized the need to quantify CG distributions beyond the visual depictions provided by spatial maps. Therefore, Florida was divided into four regions (northwest, northeast, central, and south; Fig. 1) to further evaluate seasonal and regional patterns. These regions were selected to allow direct quantitative comparisons between the panhandle and peninsula regions, and to examine differences within these regions.

Increased NLDN sensitivity following the recent upgrade apparently has enhanced the tendency for IC flashes to be misclassified as weak +CG reports (Cummins and Murphy 2009). As a result, all +CG reports with I_p less than 15 kA have been classified as IC since April 2006 (Cummins and Murphy 2009). Although there does not appear to be a unique threshold for classifying a small-positive report as a true +CG return stroke, an I_p of 15 kA appears to be the value where the number of false reports equals the number of correct reports (Biagi et al. 2007). Therefore, we separated +CG reports into three groups for detailed analysis, weak +CG (10–15 kA), ambiguous +CG (15–20 kA), and strong +CG (>20 kA). Since weak +CG reports (<15 kA) are no longer reported as +CG by the NLDN, our weak +CG analysis only examines the influence and distribution of +CG reports during 2002–06 instead of the main study period (2004–09).

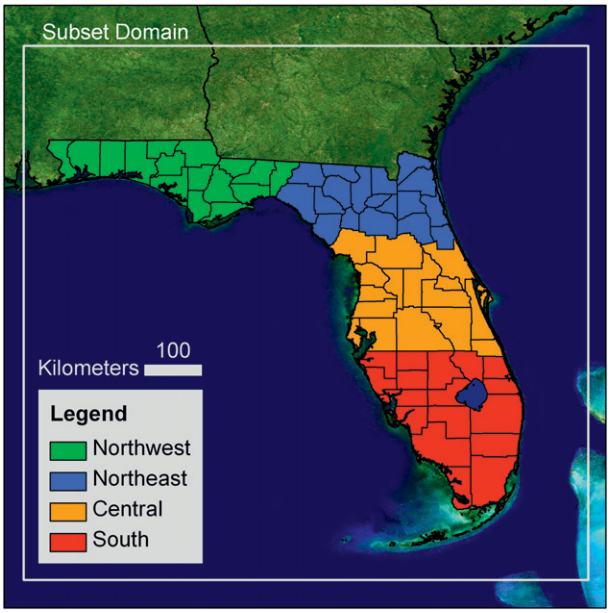

FIG. 1. The domain used to examine CG distributions in Florida, and four subset regions (northwest, northeast, central, and south) that were used to investigate seasonal and regional variability in the polarity, multiplicity, and I_p of CG flashes.

TABLE 1. Radar parameters computed by merging WSR-88D (radar) data with 20-km RUC hourly analyses in WDSS-II. These parameters then were overlaid with CG data and tracked within individual storms to examine storm-scale relationships between lightning and radar parameters. Note that "Avg" corresponds to the average of all grid cell values within a WDSS-II defined storm, while "max" corresponds to the maximum grid cell value within each storm.

Merged radar–RUC parameters
Avg reflectivity between −20° and 0°C
Avg/max reflectivity at −10°C
Avg/max reflectivity at −20°C
Avg/max reflectivity at 0°C
Avg reflectivity below 0°C
Height of 30-dBZ echo above −10°C
Height of 50-dBZ echo above −20°C
Height of 50-dBZ echo above 0°C
Height of max reflectivity
Height of 18-dBZ echo top
Height of 30-dBZ echo top
Height of 50-dBZ echo top
Max reflectivity
Avg reflectivity
Max VIL

Additional data sources were examined to describe both the atmospheric conditions and storm-scale structures associated with variability in the CG patterns. Composite rawinsonde soundings were used to describe moisture, stability, and wind shear profiles, as well as the heights of various isotherm levels. Soundings were obtained from Tallahassee (TAE), Jacksonville (JAX), Tampa (TBW), and Miami (MFL) for all days during the main study period (2004–09). Each of the 1200 UTC soundings was processed individually and then averaged to describe mean conditions for each location–region during both seasons.

The Warning Decision Support System-Integrated Information (WDSS-II; Lakshmanan et al. 2007) software was used to examine lightning, radar, and model-derived information. These data sources were combined using WDSS-II to investigate storms that produced both wildfire ignitions and severe weather. Again using WDSS-II, many 3D radar parameters (Table 1) were computed by merging data (Lakshmanan et al. 2006) from the Weather Surveillance Radar-1988 Doppler (WSR-88Ds) in Tallahassee, Jacksonville, Tampa, Melbourne, and Miami, Florida, with hourly analyses from the 20-km version of the Rapid Update Cycle (RUC; Benjamin et al. 2004) mesoscale model. We also created 2 km × 2 km grids of +CG percentage, and total CG, +CG, and −CG flash density, multiplicity, and I_p for our WDSS-II analysis.

Lightning and radar parameters were examined in individual storms using a WDSS-II algorithm (w2segmotion) that identifies and tracks mesoscale features (Lakshmanan et al. 2009) and extracts information from additional gridded fields (Lakshmanan and Smith 2009). This w2segmotion algorithm is a modification of a common image processing technique (i.e., watershed transform) that identifies local maxima and regions of support (i.e., foothills) based on user-defined thresholds (Lakshmanan et al. 2009). Rudlosky and Fuelberg (2009) present additional details on the use of WDSS-II to identify, track, and data mine storm features.

Our previous WDSS-II procedures (Rudlosky and Fuelberg 2009) were modified to investigate storms specifically in the north Florida and south Georgia regions on 13–14 May 2007. Many combinations of parameters and thresholds were examined to determine which best isolated discrete storms, and vertically integrated liquid (VIL) was found to give the best results. The maxima and range of the VIL signatures were found to be different for storms in the northern and southern regions, requiring the use of separate thresholds to best identify discrete features in each region (Table 2).

The following paragraph describes the WDSS-II algorithm (w2segmotion; Lakshmanan et al. 2006) that was used to track storms in the northern and southern regions. We use values for the northern region (Table 2) as an example to describe these procedures. The WDSS-II algorithm first searches for one or more maxima in the defined field (i.e., VIL). Maxima are defined if their area-averaged VIL exceeds 55 kg m^{-2}. The algorithm's threshold then decreases by 1 increment (10 kg m^{-2}) to

TABLE 2. User-defined thresholds for the WDSS-II algorithm (w2segmotion) that is used to data mine lightning and radar information (Lakshmanan et al. 2009). The maxima and spread of the VIL signatures differ for storms in the northern and southern regions, requiring use of separate thresholds to best identify discrete cells.

Storm region	Min, max, increment, depth VIL (kg m^{-2})	Saliency (km^2)	Smoothing filter (default)
Northern	10, 55, 10, 20	100	Median/percent
Southern	15, 60, 7.5, 30	50	Median/percent

TABLE 3. Annual total CG flash density (flashes per square kilometer per month), +CG flash density (flashes per square kilometer per month), and +CG percentage (%) in each of Florida's subset regions (Fig. 1) during 2004–09.

Region	CG flash density	+CG flash density	Percentage positive
Northwest	0.71	0.036	5.12
Northeast	0.72	0.023	3.21
Central	1.00	0.019	1.92
South	0.95	0.017	1.82
Florida	0.87	0.023	2.65

45 kg m^{-2} and again searches for maxima, continuing the incremental search for maxima down to a minimum of 10 kg m^{-2}. Following the identification of each maximum, the algorithm then searches for regions of support surrounding each. Specifically, the algorithm decreases 1 increment (10 kg m^{-2}) from the defined maximum to a new threshold and searches for a region of support that meets the saliency criteria of 100 km^2 and exceeds the new threshold of area-averaged VIL. If a supporting region is not identified for a particular maximum, the algorithm then decreases the threshold by 1 increment and again searches for a supporting region, continuing to a maximum depth (range of VIL) of 20 kg m^{-2}. These procedures were used to create a database of each storm's lightning and radar characteristics during a specified time period. Although WDSS-defined time series of storm parameters are produced, we only present characteristics averaged over each storm's lifetime.

3. Results and discussion

a. Flash density distributions

The greatest annual CG flash densities are located in the Florida Peninsula (>0.95 flashes per square kilometer per month; Table 3). The majority of Florida's CG flashes occur during the warm season, exhibiting three local flash density maxima (Fig. 2a). Greater than 2.5 flashes per square kilometer per month occur near Tampa–St. Petersburg, Orlando, and east of Lake Okeechobee (Fig. 2a). The two maxima in central Florida that compose Florida's "lightning alley" (Fig. 2a) have been related to interactions between the east and west coast sea-breeze boundaries (Hodanish et al. 1997), locally enhanced convergence due to complex coastlines (Tampa–St. Petersburg and Cape Canaveral, Lericos et al. 2002), and urban influences (e.g., Westcott 1995). The maximum east of Lake Okeechobee (Fig. 2a) results from frequent collisions between the lake-breeze and east coast sea-breeze boundaries (Hodanish et al. 1997; Lericos et al. 2002).

Figure 2 reveals that the cool season (right panels) exhibits smaller total CG flash densities (<0.542 flashes per square kilometer per month; Fig. 2b) and +CG flash densities (<0.055 +CG flashes per square kilometer per month; Fig. 2d) than the warm season (Figs. 2a,c). During the cool season, the greatest total CG and +CG densities are located in the Florida Panhandle (Figs. 2b,d). The Florida Panhandle is expected to exhibit the greatest +CG densities and percentages since MCSs are most influential in this region. Specifically, MCSs (e.g., squall lines) produce a relatively large percentage of +CG (Zajac and Rutledge 2001) and often form during slightly drier conditions and along continental airmass boundaries. Thus, northwest Florida exhibits the greatest annual +CG flash density (0.036 +CG flashes per square kilometer per month) and percentage (5.12%), with both values decreasing southward along the peninsula (Table 3). This preference for +CG in the northwest region during both seasons (Figs. 2c,d) illustrates the influence of continental air masses in +CG production.

Composite atmospheric soundings help describe seasonal and regional differences in meteorological conditions. Average conditions for each region and season are described by composite 1200 UTC soundings (Tables 4 and 5) from Tallahassee (TAE), Jacksonville (JAX), Tampa (TBW), and Miami (MFL). The most unstable convective available potential energy (CAPE) and mixed phase CAPE (0° to −40°C) are much larger in each region during the warm season than during the cool season (Table 4). Average warm season values of most unstable CAPE exceed 1450 J kg^{-1}, whereas cool season values are less than 500 J kg^{-1}. Tables 4 and 5 show that CAPE, low-level mixing ratios, and melting level heights increase southward along the peninsula, presumably resulting in lower lifting condensation levels (LCL) and greater warm cloud depth (WCD). Table 5 reveals that the warm season also exhibits the greatest deep layer moisture. Specifically, the average relative humidity (RH) in the 850–650-hPa layer exceeds 60% during the warm season (Table 5), but is less than 40% during the cool season. Larger CAPE, greater WCD,

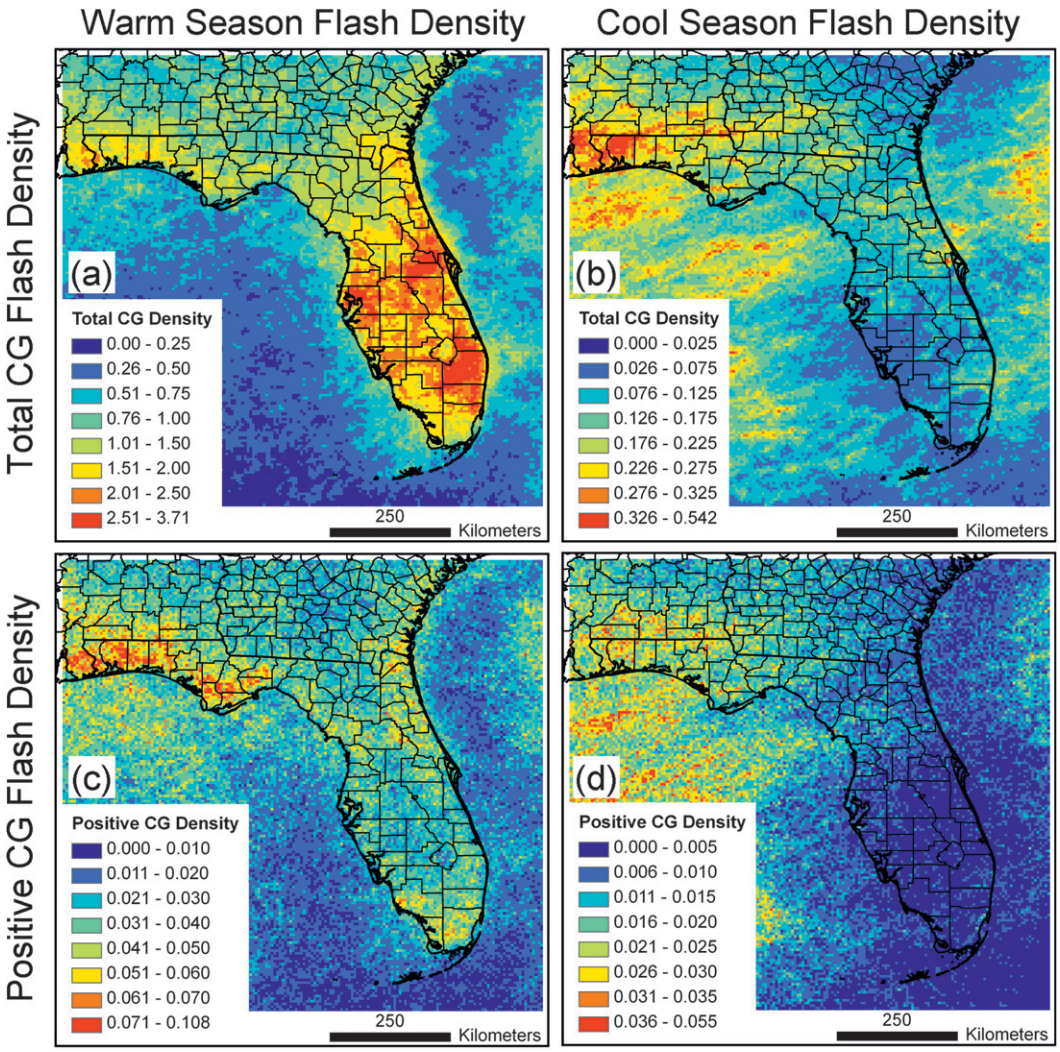

FIG. 2. (left) Warm season (May–September) and (right) cool season (October–April) CG flash densities during 2004–09 (flashes per square kilometer per month). (a) Warm season total CG, (b) cool season total CG, (c) warm season +CG, and (d) cool season +CG. Note that the color scales differ between panels.

and more deep layer moisture suggest that deep storms occur most frequently during the warm season, especially along the peninsula. Thus, the tendency for the total CG flash rate to increase with increasing cloud depth (Williams 1985) helps to explain the timing (warm season) and location (peninsula) of Florida's CG flash density maximum.

Conversely, average 0–6-km wind shear is much greater during the cool season (Table 4), especially in the northwest region (i.e., TAE). The cool season also exhibits smaller low-level mixing ratios and lower melting level heights (Table 5), which together suggest shallower WCD during the cool season. This combination of greater shear and shallower WCD previously has been related to enhanced +CG production (e.g., Brook et al. 1982; Engholm et al.1990; Carey and Buffalo 2007), and helps explain the more frequent +CG during the cool season, especially in the panhandle region.

Figure 3 further illustrates the seasonal and regional distributions of total CG (left panels) and +CG (right panels) flashes. The warm season dominates both flash density distributions (Figs. 3a,b), and the greatest warm season total CG densities occur in the central and southern regions (Fig. 3a). Although maximum annual CG densities occur in the peninsula (>0.95 flashes per square kilometer per month; Table 3), the northern regions experience the greatest percentage of cool season CG flashes (Fig. 3c). Specifically, Fig. 3c reveals that the northern regions account for as much as 87% (January), to as little as 19% (September), of Florida's total CG flashes. The northwest region also exhibits the greatest +CG flash densities during each month except September (Fig. 3b).

TABLE 4. Average 1200 UTC atmospheric conditions for each region and season during 2004–09. Composite rawinsonde soundings were created for Tallahassee (TAE), Jacksonville (JAX), Tampa (TBW), and Miami (MFL) for the cool (Oct–Apr) and warm (May–Sep) seasons. Columns display the most unstable CAPE (i.e., surface to 700 hPa; J kg^{-1}), mixed phase CAPE (0° to −40°C; J kg^{-1}), and wind shear between 0 and 6 km AGL (kt; m s^{-1}).

Location	Season	Most unstable CAPE (J kg^{-1})	Mixed phase CAPE (J kg^{-1})	Shear 0–6 km kt (m s^{-1})
TAE	Cool	125.5	38.1	40.7 (20.9)
JAX	Cool	126.2	42.0	38.2 (19.7)
TBW	Cool	247.6	83.3	35.0 (18.0)
MFL	Cool	470.9	155.4	30.2 (15.5)
TAE	Warm	1472.7	441.0	15.6 (8.0)
JAX	Warm	1450.3	332.2	15.7 (8.1)
TBW	Warm	1827.0	585.6	14.3 (7.4)
MFL	Warm	2267.7	881.3	12.9 (6.6)

Although +CG percentages are smallest during the warm season (Fig. 3d), that season exhibits the greatest +CG densities (Fig. 3b). Warm season +CG densities exceed 0.07 +CG flashes per square kilometer per month in northwest Florida, and again generally decrease southward along the peninsula (Fig. 3b). Figures 2 and 3 confirm that the CG flash density distributions vary both regionally and seasonally in Florida.

b. Cloud-to-ground characteristics

We next examine seasonal and regional trends of additional +CG and −CG characteristics (Fig. 4). Rudlosky and Fuelberg (2010) reported that the national average −CG (+CG) multiplicity increased from 2.05 (1.10) before to 2.41 (1.54) after the recent NLDN upgrade (i.e., during 2002–03). Several recent postupgrade studies have used high-speed video and electric field recording data to compare observed multiplicities with NLDN-reported values (e.g., Biagi et al. 2007; Fleenor et al. 2009). These studies found that the NLDN tends to underestimate −CG multiplicity and overestimate +CG multiplicity. Biagi et al. (2007) reported an average −CG (+CG) multiplicity of 3.71 (1.13) in southern Arizona and 2.80 (1.04) in Texas and Oklahoma, while Fleenor et al. (2009) reported a value of 3.14 (1.04) in the central Great Plains. Rudlosky and Fuelberg (2010) reported that the postupgrade −CG (+CG) multiplicity was 2.36 (1.62) in the western region (containing southern Arizona), 2.59 (1.63) in the Southeast region (including Texas and Oklahoma), and 2.11 (1.36) in the Great Plains. Despite the apparent tendency for the NLDN to underestimate (overestimate) −CG (+CG) multiplicity, both the observational studies and NLDN reports reveal similar regional variability in the CG multiplicity distributions.

Seasonal and regional CG variability is due to CG production in individual storms. Strong CG flashes often occur in intense storms, and Biagi et al. (2007) observed significant storm-to-storm variations in both average multiplicity and I_p within the same region. Most of Florida's strong −CG flashes (large multiplicity and I_p) occur during the warm season (Figs. 4c,d), often in extensive storm complexes that develop along the many sea-breeze and outflow boundaries (e.g., López and Holle 1986; Hodanish et al. 1997). Florida's greatest average +CG and −CG multiplicities occur during the warm season (Figs. 4a,c), and exceed the national averages during most months (1.54 and 2.41; Rudlosky and Fuelberg 2010). Krehbiel et al. (1979) reported that multistroke flashes become more likely as storms mature and grow in horizontal extent, which may help explain greater average warm season multiplicity. Additionally, greater −CG multiplicity in Florida has been related to larger cloud volume compared to regions farther north (Orville and Huffines 1999).

While larger cloud volume (depth and horizontal extent) helps explain greater warm season −CG multiplicity in Florida, a second possible explanation is seasonal variability in charge layer heights. Williams (2006) described the unpublished findings of Heckman (1992) who

TABLE 5. As in Table 4, but the columns contain the average melting level height (m), the mean mixing ratio in the lowest 1 km (g kg^{-1}), and the average relative humidity between 850–650 hPa (%).

Location	Season	Melting level height (m)	Mean mixing ratio (lowest 1 km) g kg^{-1}	Relative humidity (%) 850–650 hPa
TAE	Cool	3599	3.4	37.9
JAX	Cool	3590	3.6	37.9
TBW	Cool	4111	4.3	36.9
MFL	Cool	4359	5.0	38.4
TAE	Warm	4495	6.5	59.9
JAX	Warm	4523	6.6	61.3
TBW	Warm	4590	6.9	60.7
MFL	Warm	4626	7.2	60.6

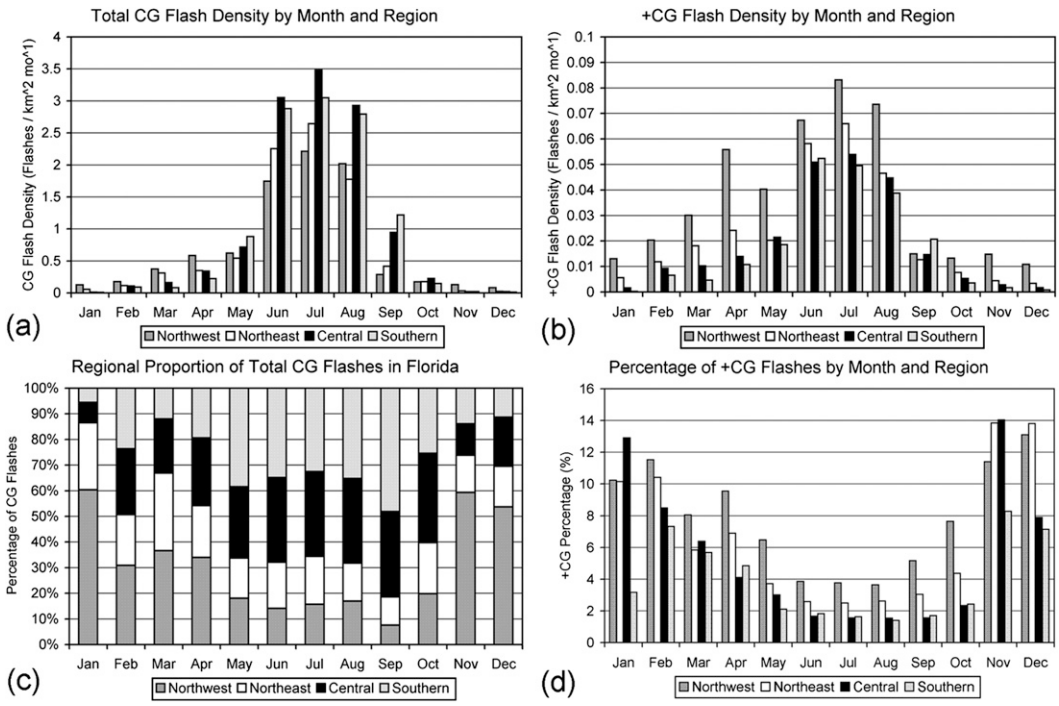

FIG. 3. Monthly values of (a) total CG flash density, (b) +CG flash density, (c) proportion of total CG flashes, and (d) percentage of +CG flashes by region (Fig. 1) during 2004–09.

offered an explanation for the number of return strokes in CG flashes. Heckman (1992) suggested that smaller interstroke currents and longer channel lengths explain the tendency for multiple return strokes in −CG flashes. Conversely, he suggested that greater interstroke currents and shorter channel lengths favor single strokes in +CG flashes. Williams (2006) noted that since charge regions are closer to the earth's surface during the cool season, CG flashes have shorter channel lengths, increasing the tendency for single-stroke behavior in both +CG and −CG flashes. Thus, longer channel lengths (i.e., higher charge regions) during the warm season in Florida also may help explain greater average −CG multiplicity.

Florida's warm season is characterized by large CAPE, deep moisture, and high melting levels (Tables 4 and 5). These conditions suggest the more frequent occurrence of strong storms with large cloud volumes and high charge regions, supporting both of the aforementioned explanations for Florida's greater warm season −CG multiplicity. One should note that −CG multiplicity and I_p follow similar seasonal trends (Figs. 4c,d), exhibiting greatest values during the warm season. Greater −CG multiplicity and I_p during Florida's warm season suggests the more frequent occurrence of strong −CG flashes, which likely dissipate the most negative charge. Interestingly, Saba et al. (2006) speculated that the occurrence of LCC (>40 ms) in −CG flashes is related to the availability of negative charge and, in turn, the horizontal extent of a thunderstorm. Although LCC is not measured by the NLDN, both the atmospheric conditions and −CG characteristics suggest a more frequent occurrence of LCC in −CG flashes during Florida's warm season.

Our focus now shifts to +CG reports, since how they are defined strongly influences their relative amount and distribution (Rudlosky and Fuelberg 2010). Rakov (2003) noted that additional knowledge about the occurrence and characteristics of +CG flashes is needed to design improved lightning protection systems. Positive CG flashes (>15 kA) exhibit their minimum multiplicity (1.3–1.7; Fig. 4a) and maximum I_p (>35 kA; Fig. 4b) during the cool season. While Florida's cool season +CG characteristics are more consistent with Rakov's (2003) definition of +CG flashes (i.e., large I_p and a single return stroke), it is unusual that +CG flashes exhibit greater multiplicity (>1.7; Fig. 4a) and smaller I_p (<35 kA; Fig. 4b) during the warm season. Reduced warm season +CG I_p suggests a greater number of ambiguous +CG reports (15–20 kA). However, since +CG flashes typically consist of a single return stroke (e.g., Rakov 2003), average warm season +CG multiplicities approaching 2 are unusual (Fig. 4a). Explanations for this finding remain unclear; however, Rudlosky and Fuelberg (2010)

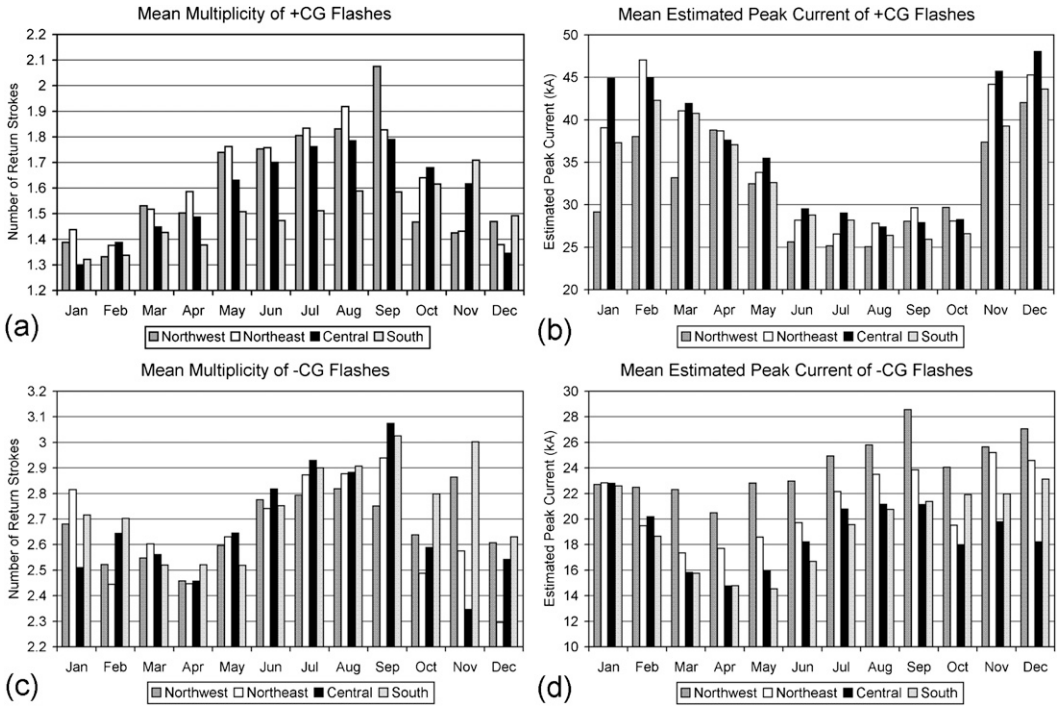

FIG. 4. Mean (a) +CG multiplicity, (b) +CG I_p, (c) −CG multiplicity, and (d) −CG I_p for each month and region (Fig. 1) during 2004–09. Note the different scales between panels and that +CG is defined by $I_p > 15$ kA.

suggested that misclassified IC flashes (e.g., Fleenor et al. 2009) and upward-propagating bipolar flashes (e.g., Rakov 2003) may contribute to the greater than unity +CG multiplicities.

Greater than unity average +CG multiplicity (Fig. 4a), seasonal +CG I_p variability (Fig. 4b), and the recent modification of the recommended weak +CG threshold (15 kA vs 10 kA) motivated an analysis of weak +CG (10–15 kA), ambiguous +CG (15–20 kA), and strong +CG (>20 kA) reports. Since the NLDN no longer reports weak +CG (<15 kA), this analysis only examines +CG reports during 2002–06. Figure 5 presents (Fig. 5a) the relative number of +CG reports in each of the three intensity groups, (Fig. 5b) the monthly percentage of +CG reports that exhibit a single return stroke, and (Fig. 5c) the monthly percentage of +CG reports that contain multiplicities greater than four. Greater than 25% of all +CG reports (>10 kA) are in the weak +CG range (10–15 kA) during each month (Fig. 5a), and this value exceeds 40% during June, July, August, and October. The warm season also exhibits the greatest percentage of ambiguous +CG reports (15–20 kA; ~25%; Fig. 5a), suggesting their increased influence on warm season +CG distributions, despite our use of the new 15-kA threshold. Conversely, the cool season exhibits the greatest percentage of strong +CG flashes (>20 kA; ~50%; Fig. 5a), and in turn the more classic +CG characteristics of smaller multiplicity and greater I_p (Figs. 4a,b). The variability in these distributions provides further evidence that the weak +CG threshold is both seasonally and regionally dependent (e.g., Biagi et al. 2007). Thus, caution must be taken to account for variations in the distribution of ambiguous +CG reports, and future video-based studies should seek to better classify weak +CG reports as being IC or CG.

The warm season surprisingly exhibits both the maximum +CG multiplicity (Fig. 4a) and the greatest percentage of weak and ambiguous +CG reports (10–20 kA; >65%; Fig. 5a). Weak and ambiguous +CG reports (10–20 kA) exhibit the greatest single-stroke percentages (Fig. 5b) and the smallest percentage with multiplicity greater than 4 (Fig. 5c). Thus, more frequent ambiguous +CG reports can help explain the smaller warm season single-stroke percentage (<75%, Fig. 5b), but they cannot explain the greater percentage of +CG reports with multiplicity greater than four (>5%, Fig. 5c). Average +CG multiplicities exceeding 1.7 during the warm season (Fig. 4a) appear to be associated with stronger +CG reports (>20 kA), not ambiguous +CG (15–20 kA). Additionally, single-stroke reports account for 65%–85% of all +CG reports (Fig. 5b). Thus, it appears that the relatively few large multiplicity +CG reports (>4 return strokes; 2%–12%; Fig. 5c) are responsible for the unusually large warm season +CG multiplicities (Fig. 4a).

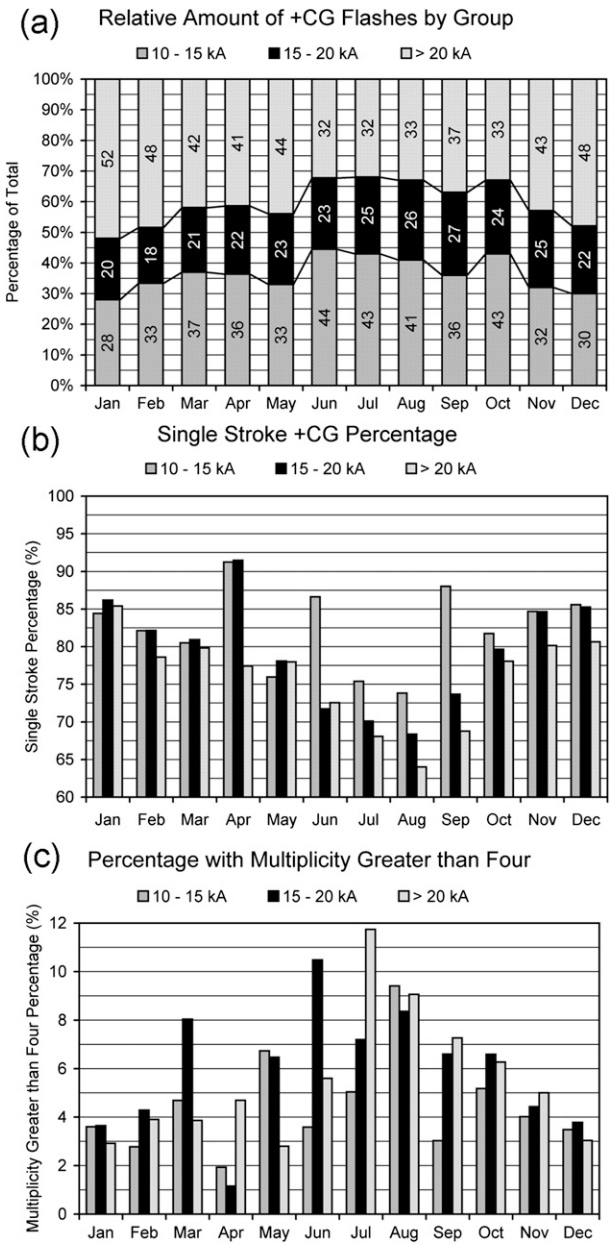

FIG. 5. Seasonal distributions of +CG reports that are subset by I_p into 3 groups, weak +CG (10–15 kA), ambiguous +CG (15–20 kA), and strong +CG (>20 kA). (a) The relative number of +CG flashes in each group during each month, (b) the monthly percentage of +CG flashes that contain 1 return stroke, and (c) the monthly percentage of +CG flashes with ≥4 return strokes. Since weak +CG flashes (10–15 kA) are no longer reported as being +CG by the NLDN, this analysis only examines +CG reports during 2002–06.

The physical properties of +CG flashes, the complex nature of Florida's convection, and the increased postupgrade NLDN sensitivity (Cummins and Murphy 2009) likely combine to explain the greater number of large multiplicity +CG reports during the warm season in Florida. Rakov and Uman (2003, p. 222) noted that +CG discharges can be initiated by branches of extensive cloud discharges, and that +CG return strokes often are preceded by significant IC discharge activity that typically lasts in excess of 100 (Fuquay 1982) or 200 ms (Rust et al. 1981). Additionally, Rakov (2003) documented an upward bipolar flash that appeared to be associated with a branch of large horizontal extent below the cloud. Krehbiel (1981) also documented three +CG flashes in Florida that apparently involved, or were the by-product of long (longer than 40 km) horizontal lightning discharges that effectively removed positive charge from a layer near the 0°C level where frozen precipitation was melting (from a region considerably below the main positive charge; Rakov 2003). We suggest that increased IC activity in the lower positive charge layer during Florida's warm season complicates the classification of +CG reports as being IC or CG. Additional research will be required to determine if this helps explain our observation of more weak and ambiguous +CG reports during the warm season; however, should it be true, it is plausible that the NLDN may misclassify the extensive horizontal IC channels often associated with true +CG flashes as being additional +CG return strokes.

Several recent field studies in Brazil have addressed the influence of measurement capabilities on our understanding of CG multiplicity (Saba et al. 2007; S10). Saba et al. (2007) used high-speed video, electric field measurements, and a lightning location system (LLS) to show that CG multiplicity is influenced by the instrumentation used to monitor it. High-speed video often is able to differentiate true CG return strokes from other lightning processes that contribute to the recorded waveforms (e.g., IC discharges and M components). For example, Saba et al. (2007) examined a single-stroke −CG flash measured by high-speed photography in which the LLS reported its multiplicity as being 4, while the multiplicity would have exceeded 6 if monitored only by an electric field recording system. Interestingly, some pulses produced by cloud discharges have wave forms that differ little from those of +CG return strokes (Rakov and Uman 2003, p. 228). This suggests that the initial IC pulses of a multistroke −CG flash could be misclassified as the initial +CG return stroke, which then is reported to contain multiple return strokes. These previous studies have demonstrated the complex nature of CG flashes and the influence of the equipment that is used to monitor them. Thus, future research on +CG distributions should examine individual CG stroke data to account for the misclassification of IC flashes as weak +CG reports.

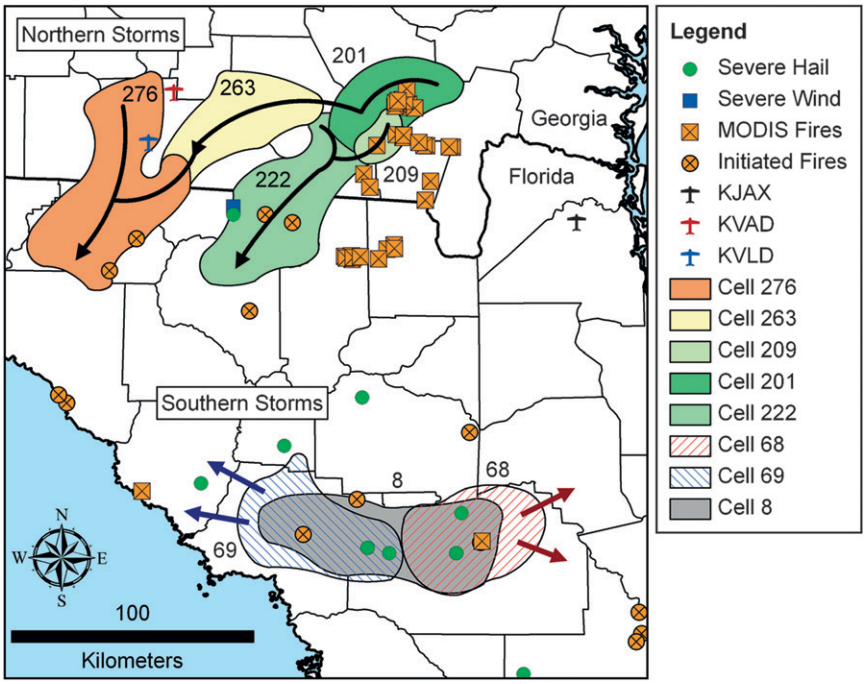

FIG. 6. Overview of the case study on 13–14 May 2007. Colored regions illustrate the areas influenced by the WDSS-II-defined storms throughout their durations (Table 7): orange squares correspond to active wildfires reported by the MODIS sensor, orange circles denote lightning-induced wildfires reported in the Florida Division of Forestry wildfire database (data not available in Georgia), and aircraft symbols correspond to Jacksonville Regional Airport (KJAX; black), Moody Air Force Base (KVAD; red), and Valdosta Regional Airport (KVLD; blue). Note that additional storms also occur in each region (not discussed), and that both regions of storms produced severe weather and ignited wildfires.

While 65%–85% of all +CG NLDN reports in Florida contain a single return stroke (Fig. 5b), our monthly averaged +CG multiplicities range from 1.3 to 2.1 (Fig. 4a). Based on high-speed video and an LLS in Brazil, S10 determined that 81% of +CG flashes consisted of a single return stroke, and that all but one subsequent stroke of the multistroke +CG flashes created a new ground contact. Furthermore, S10 found that most (75%) of the subsequent +CG strokes occurred at distances greater than 10 km from the original strike location. One should note that the NLDN currently uses a distance of 10 km to group strokes into flashes (Cummins et al. 1998), suggesting that true multistroke +CG flashes are even less likely to be reported as such by the NLDN. Interestingly, S10 also reported that some +CG strokes produced a new ground contact while the CC from a previous stroke was still in progress. Positive downward leaders also can be initiated by the CC phase of IC discharges (e.g., Kong et al. 2008). S10 concluded that the spatial and temporal criteria presently used to group −CG strokes into flashes may not be valid for +CG, and that the very concept of a lightning flash being a group of strokes that are collocated in space and time should be reconsidered for +CG. Despite the new weak +CG threshold (15 kA), Florida's unusual warm season +CG characteristics provide further evidence that the present NLDN definition of +CG flashes remains less than ideal.

c. *Case study of 13–14 May 2007*

The following case study illustrates some of the storm-scale processes that are behind the climatological patterns just described. Several factors combined on 13–14 May 2007 to produce strong +CG and −CG flashes, severe wind and hail, and natural wildfires over south Georgia and north Florida. Much of Florida was experiencing a severe drought as a decaying cold front approached the south Georgia–north Florida region. RUC hourly analyses revealed that the cold front was still apparent in the lower troposphere but had mixed out at the surface (not shown). Florida's east and west coast sea-breeze circulations dominated the low-level flow, resulting in strong convergence along the peninsula. Convergence between the east and west coast sea breezes initiated a group of storms north of Tampa at ~1800 UTC (southern storms; cells 8, 68, and 69; Fig. 6). Conversely, storms

TABLE 6. WDSS-derived near-storm environment parameters corresponding to each storm cell in the northern and southern regions. Values are from the 20-km hourly RUC analyses that precede each storm's initiation at the grid cell of that initiation. Columns display the LCL height (m), melting level height (m), most unstable CAPE (J kg^{-1}), mean mixing ratio in the lowest 1 km (g kg^{-1}), and dewpoint depression at 500 hPa (°C).

Northern storms	LCL height	Melting level height	Most unstable CAPE	Mean mixing ratio (0–1 km)	Dewpoint depression (500 hPa)
Cell 201	1198	4107	1122	10.6	16.5
Cell 209	1238	4077	1676	11.0	14.2
Cell 222	1556	4042	1965	10.7	15.9
Cell 263	1189	3993	978	11.3	18.5
Cell 276	2204	3957	820	10.4	22.2
Southern storms	**LCL height**	**Melting level height**	**Most unstable CAPE**	**Mean mixing ratio (0–1 km)**	**Dewpoint depression (500 hPa)**
Cell 8	1090	3801	3017	13.6	5.8
Cell 68	1478	3940	2097	13.1	2.5
Cell 69	865	4070	1690	13.5	0.8

formed along the Florida–Georgia border at ~2200 UTC (northeastern storms; cells 201, 209, and 222; Fig. 6) as the east coast sea breeze interacted with the decaying cold front and an active wildfire complex. Farther west, northerly flow converged with the Gulf Coast sea breeze to initiate additional storms.

The northern storms (i.e., northwestern and northeastern) likely ingested smoke from preexisting wildfires (Fig. 6). These fires began on 16 April and had expanded into an extensive complex located in southeast Georgia and north Florida (Fig. 6). Smoke produced by these fires influenced large portions of the Southeast throughout April, May, and June 2007. Their smoke was clearly evident in Moderate Resolution Imaging Spectroradiometer (MODIS) imagery of the area (not shown). Although MODIS imagery was not available during 13–14 May 2007, the widespread smoke during the preceding weeks along with easterly low-level flow (below 1 km) suggest that the northern storms were influenced by smoke. Specifically, the east coast sea breeze strengthened low-level easterly flow just prior to initiation of the storms nearest the fires. Smoke was observed throughout the period at Valdosta Regional Airport (KVLD; Fig. 6), between 1400–1800 UTC at Moody Air Force Base (KVAD), and during 2000–0000 UTC at Jacksonville Regional Airport (KJAX). Thus, it is likely that each of the northern storms ingested smoke, but that the storms farthest from the active fires likely ingested smaller amounts.

The northern and southern regions of storms (Fig. 6) developed under different environmental conditions (Table 6). Although the LCL and melting level heights are comparable between regions (Table 6), the greatest most unstable CAPE is located in the southern region. The lower levels are slightly drier in the north, with mean low-level (0–1 km) mixing ratios of ~11 g kg^{-1} (Table 6) compared with ~13 g kg^{-1} in the south. The greatest difference between regions is the amount of midlevel moisture (Table 6). Specifically, the north is notably drier in the middle levels, exhibiting much greater 500-hPa dewpoint depressions (>14.2°C; Table 6) than the south (<6°C). While the atmospheric conditions in the north are common during Florida's transition from the cool to warm seasons, conditions in the south are most common during Florida's warm season.

The southern storms, characteristic of Florida's warm season, produce predominately −CG flashes (Table 7; Fig. 7a) and exhibit 30 dBZ (50 dBZ) echo tops above 15 km (9 km; Table 8). Figure 6 illustrates the areas influenced by the WDSS-II-defined storms throughout their durations (Table 7). Animations reveal that the most intense southern storm (cell 8; Fig. 6) begins at 1757 UTC, remains nearly stationary, and initially consists of two main cores. The separate cores eventually split into cells 68 and 69 at 1955 UTC, which then track toward the west and east, respectively (Fig. 6). Storm tracks are evident in the clustering of strong −CG flashes (Fig. 7a), and strong −CG flashes also are clustered near the two hail reports in cell 8. The southern storms produce the smallest +CG percentages (<3%; Table 7), and their +CG distribution is widely varied (Fig. 7a).

Lightning characteristics in several of the northern storms (Fig. 7b) are opposite those of the southern storms (Fig. 7a), with clusters of +CG and more sporadic −CG. Although +CG flashes typically occur outside areas with significant updrafts (Kopp and Orville 1987), they sometimes cluster in the cores of strong storms (MacGorman and Burgess 1994). These reversed-polarity (+CG dominated) storms are most common in relatively dry environments with high cloud bases and shallow warm

TABLE 7. Average WDSS-II-derived lightning characteristics and duration of each of the northern and southern storms. Values represent the average of all 1-min storm values during each storm's entire duration. Columns also display the average +CG percentage, and +CG (−CG) multiplicity, and I_p for the northern (southern) storms.

Northern storms	Duration (h:min)	Percentage positive (%)	+CG multiplicity	+CG peak current
Cell 201	1:15	54.7	1.54	64.5
Cell 209	0:36	69.7	1.10	57.8
Cell 222	2:24	44.7	1.01	53.0
Cell 263	1:26	13.7	1.00	35.3
Cell 276	2:32	5.0	2.61	31.0
Southern Storms	**Duration (h:min)**	**Percentage positive (%)**	**−CG multiplicity**	**−CG peak current**
Cell 8	1:58	1.9	2.46	−14.2
Cell 68	1:06	1.2	3.26	−18.4
Cell 69	1:02	2.3	2.54	−14.7

cloud depths (e.g., Carey and Buffalo 2007). Interestingly, large +CG percentages have also been observed in thunderstorms that ingest smoke from wildfires during drought conditions (e.g., Vonnegut et al. 1995; Lyons et al. 1998b; Murray et al. 2000; Lang and Rutledge 2006; Wang et al. 2009). Smoke-enhanced +CG has been observed in pyrocumulus clouds directly associated with the source fires (Vonnegut et al. 1995) and in storms at long distances downwind from the source fires (Lyons et al. 1998b). This is an important relationship since +CG flashes often exhibit the unique combination of large peak current and LCC (Saba et al. 2006), and thus are prime candidates for igniting subsequent wildfires (Fuquay et al. 1972).

Since the atmosphere is drier to the north, especially in the middle levels (Table 6), these storms produce strong outflow boundaries that yield complex storm evolutions. Figure 6 illustrates the areas influenced by the WDSS-II-defined storms, revealing that the northern storms undergo several splits and mergers. Figure 7b illustrates clear differences in the lightning production of the northern storms. Specifically, the northern storms nearest the active wildfires (cells 201, 209, and 222) produce predominately strong +CG flashes (Fig. 7b), whereas the storms farthest west (cells 263 and 276) produce predominately −CG. Both groups of storms (west and east) ignite wildfires (Fig. 6), and a +CG-dominated storm (cell 222) also produces severe wind and hail.

Although the northern storms that are farthest from the active wildfires (cells 263 and 276; Fig. 6) exhibit greater +CG percentages than the southern storms (Table 7), they exhibit smaller +CG percentages than the storms farther east. Figure 6 reveals that cell 263 actually begins as cell 201 and eventually merges into cell 276. Cell 263 exhibits a greater average +CG percentage than cell 276 (13.7% versus 5%; Table 7), likely because it originated as a +CG-dominated storm. The northwestern storms (i.e., those farthest from the fires; cells 263 and 276) exhibit the lowest average 50-dBZ echo tops and greatest average reflectivity below 0°C (Table 8). These observations suggest precipitation loading and relatively weak updrafts.

Conversely, the northeastern storms (201, 209, and 222; Fig. 6) originate either directly above or just west of the existing wildfires. These storms produce predominately +CG (Table 7) and an average I_p (>50 kA) that is much greater than climatology (Fig. 4b). These storms develop in a drier environment than the southern storms, and exhibit the smallest average reflectivity below 0°C (Table 8). Rosenfeld et al. (2007) suggested that the combination of heat and smoke from intense wildfires is associated with a high concentration of small droplets that ascend rapidly in strong updrafts. Thus, the +CG-dominated storms (cells 201, 209, and 222) also exhibit the highest average 30-dBZ echo tops (Table 8) and the greatest average 30-dBZ echo heights above −10°C. Increased competition for cloud condensation nuclei and the strength of the updrafts likely lead to a greater quantity of supercooled liquid water at higher levels (i.e., colder temperatures; Rosenfeld et al. 2007). Greater supercooled liquid water content in the mixed phase region (0° to −40°C) appears to be the common link between reversed-polarity (+CG dominated) storms in the Great Plains (e.g., Williams et al. 2005; Carey and Buffalo 2007) and those associated with smoke ingestion during drought conditions (e.g., Lang and Rutledge 2006).

The northeastern storms (cells 201, 209, and 222) provide additional examples of reversed-polarity (+CG dominated) storms that appear to ingest smoke during drought conditions, produce predominately strong +CG flashes, and ignite subsequent wildfires (e.g., Lang and Rutledge 2006). Lyons et al. (1998b) suggested that the increased number of strong +CG flashes in reversed-polarity storms may indicate that the charge that normally

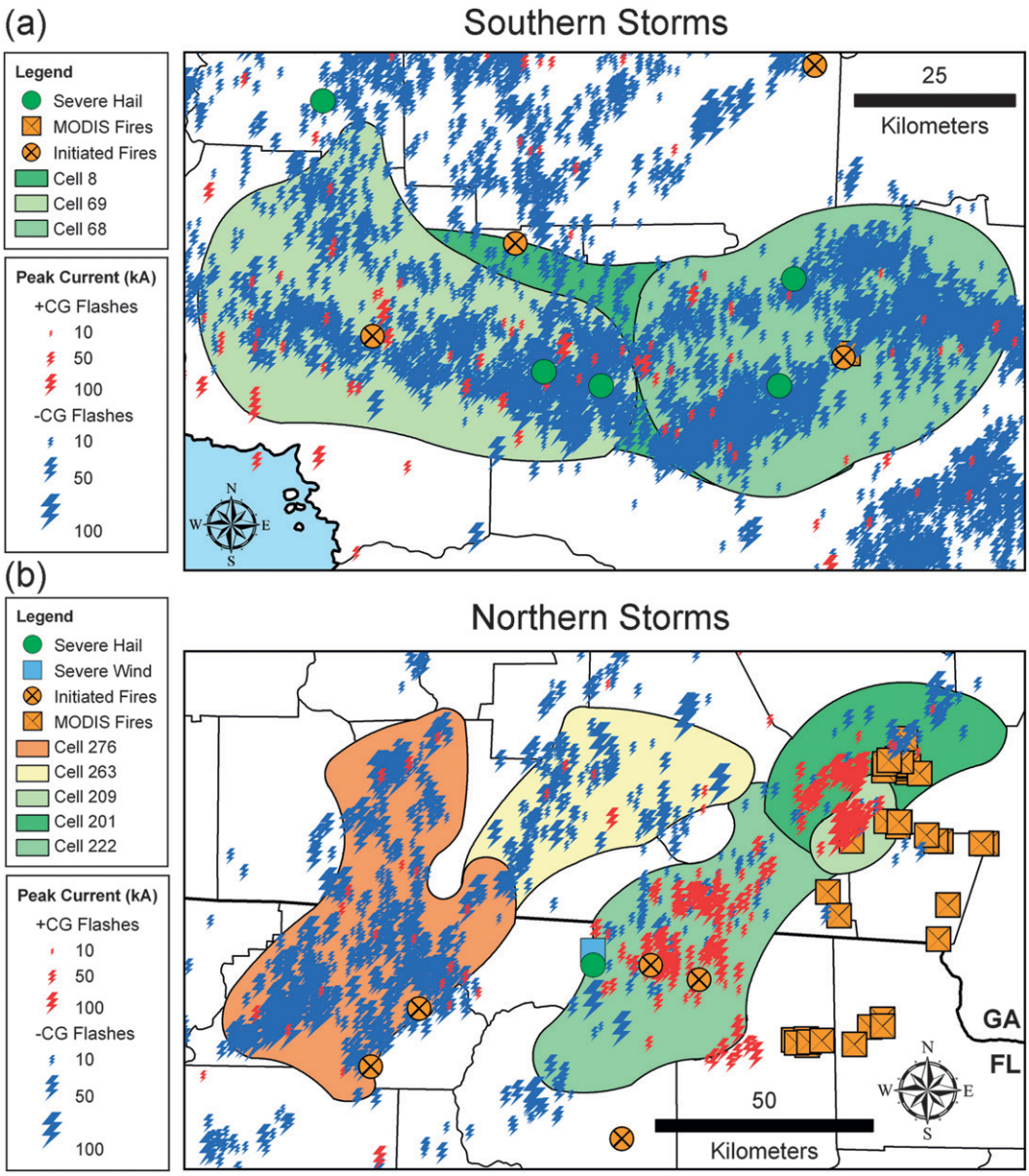

FIG. 7. Overview of the (a) southern and (b) northern storm regions. Note that additional storms also occur in each region but are not discussed. Colored regions illustrate the areas influenced by the WDSS-II defined storms throughout their durations (Table 7): orange squares correspond to active wildfires reported by the MODIS sensor, orange circles represent lightning-induced wildfires reported in the Florida Division of Forestry wildfire database (data not available in Georgia), and the blue and red bolt symbols represent −CG and +CG flashes, respectively. The size of the bolt symbols corresponds to the I_p of the CG flashes.

participates in IC flashes somehow has been reapportioned into the +CG formation process. This may help explain the strength (large I_p) of +CG flashes in reversed-polarity storms (Table 7). However, analysis of IC data sources will be required to quantify any relationships between +CG characteristics and IC activity in reversed-polarity storms.

GIS analysis reveals that the main northern storm (cell 222) produces a cluster of strong +CG flashes that ignite a subsequent wildfire at ~0000 UTC, nearly coincident in time with severe hail and wind reports (Fig. 6). Although −CG flashes greatly outnumber +CG flashes, and likely are responsible for most natural wildfire ignitions, this example provides further evidence that storms that ingest smoke during drought conditions may ignite a disproportionate number of wildfires. We note this apparent self-perpetuating nature

TABLE 8. Average WDSS-II-derived radar characteristics for each of the northern and southern storms. Values represent the average of all 1-min storm values during each storm's entire duration. Columns display average echo tops defined by the maximum height of the 30- and 50-dBZ echoes, the average height of the 30-dBZ echo top above the −10°C isotherm, the average height of the 50-dBZ echo above the melting level (0°C), and the average reflectivity below the melting level.

Northern storms	Echo top 30 dBZ	Height of 30 dBZ above −10°C (km)	Echo top 50 dBZ	Height of 50 dBZ above 0°C (km)	Reflectivity below 0°C (dBZ)
Cell 201	17.0	5.6	8.5	1.9	32.3
Cell 209	16.2	5.0	7.3	1.4	31.9
Cell 222	15.6	3.8	6.7	1.3	36.4
Cell 263	15.2	3.4	6.0	0.9	38.9
Cell 276	14.6	3.2	6.3	1.0	38.1
Southern storms	**Echo top 30 dBZ**	**Height of 30 dBZ above −10°C (km)**	**Echo top 50 dBZ**	**Height of 50 dBZ above 0°C (km)**	**Reflectivity below 0°C (dBZ)**
Cell 8	15.3	4.3	9.9	2.6	33.1
Cell 68	16.9	4.3	9.8	2.1	32.3
Cell 69	14.9	3.4	9.3	2.0	34.5

of wildfires and +CG lightning, and suggest that additional knowledge of these relationships may provide forestry officials additional lead time for distributing resources.

These case study findings further suggest that CG characteristics describe the variability in thunderstorm charging and the relative charge dissipation roles of +CG and −CG flashes in individual storms. For example, strong storms in both the northern and southern regions are characterized by high echo tops, large CG flash rates, and strong CG flashes. Although both groups of storms likely produce similar quantities of charge, the polarity of the charge generated and dissipated appears to be influenced by the near-storm environment. These results further indicate that intense storms contain strong CG flashes that are either +CG or −CG based on the atmospheric conditions. This supports the suggestion of Orville et al. (2002) that the key factors determining charge in the lower portion of the lightning channel are related to the total charge available for producing a flash. Thus, future studies should continue to examine relationships between strong CG flashes, severe storms, structural damage, and wildfire ignitions to help identify potential forecasting and nowcasting applications.

4. Summary and conclusions

We have shown that Florida's cloud-to-ground (CG) lightning characteristics vary by region and season because of differences in atmospheric conditions and their influence on CG production in individual storms. These findings further suggest that CG characteristics can provide valuable information to decision makers regarding the CG threat. Specifically, certain atmospheric conditions produce intense storms with strong CG flashes whose polarity, multiplicity, and estimated peak current I_p depend on the near-storm environment. Thus, positive CG (+CG) and negative CG (−CG) characteristics appear to be indicative of the amount and type of charge generated and dissipated in individual storms. The combination of CG characteristics and other measures of storm intensity (e.g., radar parameters) allow detailed analysis of patterns and trends that suggest increased structural damage, wildfire ignitions, and/or severe storms.

Florida's greatest total CG (+CG) flash densities occur during the warm season, especially over the peninsula (panhandle). Conversely, the warm season exhibits the smallest +CG percentages. This observation suggests the tendency for the +CG flash rate to decrease with increasing cloud depth (e.g., Rakov 2003). Florida's deepest storms occur most frequently during the warm season, producing the greatest average −CG flash density, multiplicity, and I_p. Our findings suggest that −CG characteristics are directly related on the seasonal and regional scales, and may be indicative of storm depth, extent, and intensity. Specifically, greater −CG multiplicity and I_p during Florida's warm season are likely related to greater cloud extent (Krehbiel et al. 1979), larger cloud volume (Orville and Huffines 1999), and higher charge layers (e.g., Williams 2006).

Warm season +CG characteristics were found to be unusual, exhibiting large multiplicity (>1.7) and small I_p (<35 kA). During the warm season, weak +CG reports (10–15 kA) account for greater than 40% of all +CG in Florida, and ~25% of +CG reports are in the ambiguous +CG range (15–20 kA). Although relatively small average +CG I_p during the warm season can be attributed to an increased number of ambiguous +CG reports (15–20 kA), strong +CG reports (>20 kA) appear to be responsible for the greater warm season +CG multiplicity. Since +CG flashes typically consist of a single

return stroke (Rakov 2003), and weak +CG reports are even more likely to have a single return stroke, we suggest that our findings are a result of both the measurement capabilities and physical characteristics of +CG flashes in Florida.

Our findings further demonstrate the complexities of +CG flashes and the influence of the measurement capabilities. The National Lightning Detection Network (NLDN) tends to overestimate the multiplicity of +CG flashes, even more so following the recent upgrade. It appears that portions of intracloud (IC) channels might be misclassified as +CG return strokes; however, a combination of IC and video-based studies will be required to document this potential relationship. Interestingly, S10 noted that the spatial and temporal criteria presently used to group −CG strokes into flashes may not be valid for +CG, and that the very concept of a lightning flash being a group of strokes that are collocated in space and time should be reconsidered for +CG. As demonstrated by Florida's unusual warm season +CG characteristics, it is clear that the present NLDN definition of +CG flashes remains less than ideal.

Conversely, +CG flashes were found to have more classic characteristics during the cool season, exhibiting relatively small multiplicity (1.3–1.7) and large I_p (>35 kA). Enhanced cool season +CG production has been attributed to greater shear and drier conditions compared to the warm season. Also, cool season thunderstorms generally are associated with synoptic-scale systems that produce relatively large +CG percentages (e.g., Zajac and Rutledge 2001). Within Florida, the panhandle exhibits the greatest annual +CG densities and percentages, with both values decreasing southward along the peninsula. The panhandle also exhibits the smallest average +CG multiplicity and greatest average +CG I_p, suggesting more true +CG flashes (vs ambiguous or misclassified +CG reports) in this region.

We documented two regions of storms on 13–14 May 2007 that developed under different atmospheric conditions and exhibited dissimilar CG patterns. Both regions of storms produced severe weather and ignited wildfires. Several northern storms contained predominately strong +CG flashes, whereas the southern storms produced predominately strong −CG. The southern storms developed along sea-breeze and outflow boundaries in a moist environment, producing predominately −CG flashes, severe hail reports, and wildfire ignitions. Although the southern storms were characteristic of Florida's warm season, the northern storms formed in a slightly drier environment and also ingested smoke from existing wildfires.

The northern storms nearest the wildfires (northeastern storms) produced predominately strong +CG flashes, whereas the northern storms farthest from the fires (northwestern storms) produced mostly −CG. Thus, smoke ingestion during dry conditions was not sufficient to explain the occurrence of the reversed-polarity (+CG dominated) storms. Only the northern storms nearest the fires exhibited high echo tops comparable to those of the −CG-dominated southern storms. It appears that the heat and smoke very near the fires were necessary for the reversed-polarity storms. These storms produced frequent and strong +CG flashes that are more likely to ignite subsequent wildfires (e.g., Latham and Williams 2001). We note this apparent self-perpetuating relationship between wildfires and strong +CG flashes, and suggest that knowledge of the mesoscale environment can lead to a better diagnosis of the CG threat, and improved information for wildfire managers.

Our findings illustrate the dependence of CG characteristics on the near-storm environment through storm-scale processes. Additional research on this topic is needed to fully exploit the extensive information contained in the NLDN archive. Intracloud (IC) lightning detection technologies will continue to provide new perspectives on CG patterns. For example, the Lightning Detection and Ranging (LDAR) and Lightning Mapping Array (LMA) networks are advancing our knowledge by quantifying the amount and type of charge that is dissipated in specific cloud layers. The upcoming Geostationary Operational Environmental Satellite-R (GOES-R) Geostationary Lightning Mapper (GLM; Goodman et al. 2008) will soon complement the NLDN to provide total lightning data to all National Weather Service (NWS) forecast offices for the first time. Therefore, the combined analysis of IC and CG flashes and their relation to specific atmospheric conditions and storm-scale processes will help provide for a smooth transition to GLM operations.

Acknowledgments. Funding for this project was provided by the Florida Power and Light Corp. and NOAA/NESDIS through the Northern Gulf Institute and the Cooperative Institute for Climate and Satellites. Additional support was provided by Vaisala, Inc., who collected the CG data and the Tallahassee National Weather Service Forecast Office who provided the NLDN data as part of our ongoing collaborations. Rapid Update Cycle data were obtained from the Atmospheric Radiation Measurement (ARM) Program sponsored by the U.S. Department of Energy, Office of Science, Office of Biological and Environmental Research, Climate and Environmental Sciences Division. Many individuals have provided valuable insights, and we specifically want to thank Phil Shafer, Geoffrey Stano, Irv Watson, Ron Holle, Ken Cummins, and Nick Demetriades for their

insights, encouragement, and support. We would also like to thank Valliappa Lakshmanan, Travis Smith, Greg Stumpf, and Kurt Hondl for their WDSS-II support. We also thank the editorial staff and anonymous reviewers for their assistance during the publication process. Finally, we would like to express our gratitude to Jim Gurka and Steve Goodman (NOAA/NESDIS) for their continuing financial support.

REFERENCES

Arritt, R. W., 1993: Effects of large-scale flow on the characteristic features of the sea breeze. *J. Appl. Meteor.,* **32,** 116–125.

Benjamin, S. G., and Coauthors, 2004: An hourly assimilation–forecast cycle: The RUC. *Mon. Wea. Rev.,* **132,** 495–518.

Biagi, C. J., K. L. Cummins, K. E. Kehoe, and E. P. Krider, 2007: National lightning detection network (NLDN) performance in southern Arizona, Texas, and Oklahoma in 2003–2004. *J. Geophys. Res.,* **112,** D05208, doi:10.1029/2006JD007341.

Brook, M., M. Nakano, P. Krehbiel, and T. Takeuti, 1982: The electrical structure of the Hokuriku winter thunderstorms. *J. Geophys. Res.,* **87** (C2), 1207–1215.

Carey, L. D., and K. M. Buffalo, 2007: Environmental control of cloud-to-ground lightning polarity in severe storms. *Mon. Wea. Rev.,* **135,** 1327–1353.

Cummins, K. L., and M. J. Murphy, 2009: An overview of lightning locating systems: History, techniques, and data uses, with an in depth look at the U.S. NLDN. *IEEE Trans. Electromagn. Compat.,* **51** (3), 499–518.

——, ——, E. A. Bardo, W. L. Hiscox, R. B. Pyle, and A. E. Pifer, 1998: A combined TOA/MDF technology upgrade of the U.S. National Lightning Detection Network. *J. Geophys. Res.,* **103** (D8), 9035–9044.

Engholm, C. D., E. R. Williams, and R. M. Dole, 1990: Meteorological and electrical conditions associated with positive cloud-to-ground lightning. *Mon. Wea. Rev.,* **118,** 470–487.

Fleenor, S. A., C. J. Biagi, K. L. Cummins, E. P. Krider, and X. M. Shao, 2009: Characteristics of cloud-to-ground lightning in warm-season thunderstorms in the Central Great Plains. *Atmos. Res.,* **91** (2–4), 333–352.

Fuquay, D. M., 1982: Positive cloud-to-ground lightning in summer thunderstorms. *J. Geophys. Res.,* **87** (C9), 7131–7140.

——, A. R. Taylor, R. G. Hawe, and C. W. Schmid, 1972: Lightning discharges that caused forest fires. *J. Geophys. Res.,* **77,** 2156–2158.

Goodman, S. J., R. J. Blakeslee, W. Koshak, W. Petersen, D. E. Buechler, P. R. Krehbiel, P. Gatlin, and S. Zubrick, 2008: Pre-launch algorithms and risk reduction in support of the Geostationary Lightning Mapper for GOES-R and beyond. Preprints, *Third Conf. on Meteorological Applications of Lightning Data,* New Orleans, LA, Amer. Meteor. Soc., P3.3. [Available online at http://ams.confex.com/ams/88Annual/techprogram/paper_129401.htm.]

Heckman, S., 1992: Why does a lightning flash have multiple strokes? Ph.D. thesis, Department of Earth, Atmospheric and Planetary Sciences, Massachusetts Institute of Technology, 134 pp.

Hodanish, S., D. Sharp, W. Collins, C. Paxton, and R. E. Orville, 1997: A 10-yr monthly lightning climatology of Florida: 1986–95. *Wea. Forecasting,* **12,** 439–448.

Knapp, D. I., 1994: Using cloud-to-ground lightning data to identify tornadic thunderstorm signatures and nowcast severe weather. *Natl. Wea. Dig.,* **19,** 35–42.

Kong, X., X. Qie, and Y. Zhao, 2008: Characteristics of downward leader in a positive cloud-to-ground lightning flash observed by high-speed video camera and electric field changes. *Geophys. Res. Lett.,* **35,** L05816, doi:10.1029/2007GL032764.

Kopp, T. J., and R. E. Orville, 1987: A case study of positive cloud-to-ground flashes in the GALE program. *Eos, Trans. Amer. Geophys. Union,* **68,** 277.

Krehbiel, P. R., 1981: An analysis of the electric field change produced by lightning. Tech. Rep. T-11, Geophysical Research Center, Institute of Mining and Technology, Socorro, NM, 245 pp.

——, M. Brook, and R. A. McCrory, 1979: An analysis of the charge structure of lightning discharges to ground. *J. Geophys. Res.,* **84,** 2432–2456.

Lakshmanan, V., and T. Smith, 2009: Data mining storm attributes from spatial grids. *J. Atmos. Oceanic Technol.,* **26,** 2353–2365.

——, ——, K. Hondl, G. J. Stumpf, and A. Witt, 2006: A real-time, three-dimensional, rapidly updating, heterogeneous radar merger technique for reflectivity, velocity, and derived products. *Wea. Forecasting,* **21,** 802–823.

——, ——, G. Stumpf, and K. Hondl, 2007: The Warning Decision Support System–Integrated Information. *Wea. Forecasting,* **22,** 596–612.

——, K. Hondl, and R. Rabin, 2009: An efficient, general-purpose technique for identifying storm cells in geospatial images. *J. Atmos. Oceanic Technol.,* **26,** 523–537.

Lang, T. J., and S. A. Rutledge, 2006: Cloud-to-ground lightning downwind of the 2002 Hayman forest fire in Colorado. *Geophys. Res. Lett.,* **33,** L03804, doi:10.1029/2005GL024608.

Latham, D., and E. Williams, 2001: Lightning and forest fires. *Forest Fires: Behavior and Ecological Effects,* E. A. Johnson and K. Miyanishi, Eds., Academic Press, 375–418.

Lericos, T. P., H. E. Fuelberg, A. I. Watson, and R. L. Holle, 2002: Warm season lightning distributions over the Florida Peninsula as related to synoptic patterns. *Wea. Forecasting,* **17,** 83–98.

López, R. E., and R. L. Holle, 1986: Diurnal and spatial variability of lightning activity in northeastern Colorado and central Florida during the summer. *Mon. Wea. Rev.,* **114,** 1288–1312.

Lyons, W. A., M. Uliasz, and T. E. Nelson, 1998a: Large peak current cloud-to-ground lightning flashes during the summer months in the contiguous United States. *Mon. Wea. Rev.,* **126,** 2217–2233.

——, T. E. Nelson, E. R. Williams, J. Cramer, and T. Turner, 1998b: Enhanced positive cloud-to-ground lightning in thunderstorms ingesting smoke from fires. *Science,* **282,** 77–81.

MacGorman, D. R., and D. W. Burgess, 1994: Positive cloud-to-ground lightning in tornadic storms and hailstorms. *Mon. Wea. Rev.,* **122,** 1671–1697.

Murray, N. D., R. E. Orville, and G. R. Huffines, 2000: Effect of pollution from Central American fires on cloud-to-ground lightning in May 1998. *Geophys. Res. Lett.,* **27,** 2249–2252.

Orville, R. E., and A. C. Silver, 1997: Lightning ground flash density in the contiguous United States: 1992–95. *Mon. Wea. Rev.,* **125,** 631–638.

——, and G. R. Huffines, 1999: Lightning ground flash measurements over the contiguous United States: 1995–97. *Mon. Wea. Rev.,* **127,** 2693–2703.

——, and ——, 2001: Cloud-to-ground lightning in the United States: NLDN results in the first decade, 1989–98. *Mon. Wea. Rev.,* **129,** 1179–1193.

——, ——, W. R. Burrows, R. L. Holle, and K. L. Cummins, 2002: The North American Lightning Detection Network

(NALDN)—First results: 1998–2000. *Mon. Wea. Rev.,* **130,** 2098–2109.

Rakov, V. A., 2003: A review of positive and bipolar lightning discharges. *Bull. Amer. Meteor. Soc.,* **84,** 767–776.

——, and M. A. Uman, 2003: *Lightning—Physics and Effects*. Cambridge University Press, 687 pp.

——, ——, and R. Thottappillil, 1994: Review of lightning properties from electric field and TV observations. *J. Geophys. Res.,* **99,** 10 745–10 750.

Reap, R. M., 1994: Analysis and prediction of lightning strike distributions associated with synoptic map types over Florida. *Mon. Wea. Rev.,* **122,** 1698–1715.

Rosenfeld, D., M. Fromm, J. Trentmann, G. Luderer, M. O. Andreae, and R. Servranckx, 2007: The Chisholm firestorms: Observed microstructure, precipitation, and lightning activity of a pyrocumulonimbus. *Atmos. Chem. Phys.,* **7,** 645–659.

Rudlosky, S. D., and H. E. Fuelberg, 2009: Utilizing WDSS-II to automate dataset preparation for a statistical investigation of total lightning and radar echoes within severe and non-severe storms. Preprints, *Fourth Conf. on Meteorological Applications of Lightning Data,* Phoenix, AZ, Amer. Meteor. Soc., P2.4. [Available online at http://ams.confex.com/ams/pdfpapers/150719.pdf.]

——, and ——, 2010: Pre- and postupgrade distributions of NLDN reported cloud-to-ground lightning characteristics in the contiguous United States. *Mon. Wea. Rev.,* **138,** 3623–3633.

Rust, W. D., D. R. MacGorman, and R. T. Arnold, 1981: Positive cloud-to-ground lightning flashes in severe storms. *Geophys. Res. Lett.,* **8,** 791–794.

Saba, M. M. F., O. Pinto Jr., and M. G. Ballarotti, 2006: Relation between lightning return stroke peak current and following continuing current. *Geophys. Res. Lett.,* **33,** L23807, doi:10.1029/2006GL027455.

——, M. G. Ballarotti, L. Z. S. Campos, and O. Pinto Jr., 2007: High-speed video observations of positive lightning. *Proc. Ninth Int. Symp. on Lightning Protection,* Foz do Iguacu, Brazil, Institute of Electrotechnics and Energy of the University of São Paulo, 5 pp. [Available online at http://ws9.iee.usp.br/sipdax/papersix/sessao01/1.5.pdf.]

Vonnegut, B., D. J. Latham, C. B. Moore, and S. J. Hunyady, 1995: An explanation for anomalous lightning from forest fire clouds. *J. Geophys. Res.,* **100,** 5037–5050.

Wang, J., S. Van den Heever, and J. S. Reid, 2009: A conceptual model for the link between Central American biomass burning aerosols and severe weather over the south central United States. *Environ. Res. Lett.,* **4,** 015003, doi:10.1088/1748-9326/4/1/015003.

Westcott, N. E., 1995: Summertime cloud-to-ground lightning activity around major Midwestern urban areas. *J. Appl. Meteor.,* **34,** 1633–1642.

Williams, E. R., 1985: Large scale charge separation in thunderclouds. *J. Geophys. Res.,* **90,** 6013–6025.

——, 2006: Problems in lightning physics—The role of polarity asymmetry. *Plasma Sources Sci. Technol.,* **15,** S91–S108, doi:10.1088/0963-0252/15/2/S12.

——, V. Mushtak, D. Rosenfeld, S. Goodman, and D. Boccippio, 2005: Thermodynamic conditions favorable to superlative thunderstorm updraft, mixed phase microphysics and lightning flash rate. *Atmos. Res.,* **76,** 288–306.

Zajac, B. A., and S. A. Rutledge, 2001: Cloud-to-ground lightning activity in the contiguous United States from 1995 to 1999. *Mon. Wea. Rev.,* **129,** 999–1019.